Glia

WILEY

GLIA

RESEARCH ARTICLE OPEN ACCESS

Disruption of Oligodendroglial Autophagy Leads to Myelin Morphological Deficits, Neuronal Apoptosis, and Cognitive Decline in Aged Mice

Niki Ktena[1,2] | Dimitrios Spyridakos[1] | Alexandros Georgilis[1,2] | Ilias Kalafatakis[1,2] | Efstathia Thomoglou[1] | Angeliki Kolaxi[3] | Vassiliki Nikoletopoulou[3] | Maria Savvaki[1] | Domna Karagogeos[1,2]

[1]School of Medicine, University of Crete, Heraklion, Greece | [2]Institute of Molecular Biology & Biotechnology—FORTH, Heraklion, Greece | [3]Department of Fundamental Neurosciences (DNF), University of Lausanne, Lausanne, Switzerland

Correspondence: Domna Karagogeos (karagoge@imbb.forth.gr)

Received: 1 November 2024 | **Revised:** 1 March 2025 | **Accepted:** 4 March 2025

Funding: This work was supported by funding from the Hellenic Foundation for Research and Innovation (HFRI grant agreements 1676 [to M.S.] and 14772 [to D.K.]), the National Recovery and Resilience Plan Greece 2.0, funded by the European Union—Next Generation EU, Proposal TAEDR 0535850 (to D.K.), the National Multiple Sclerosis Society (NMSS, pilot Research Grant, PP-1809-32556 to M.S.), the State Scholarships Foundation (IKY, in the context of the project "Strengthening Human Resources Research Potential via Doctorate Research," MIS-5113934), the Hellenic Academy of Neuroimmunology (HELANI) and the Manassaki scholarship of the University of Crete (to N.K.).

Keywords: aging | autophagy | CNS | myelin | neurodegeneration

ABSTRACT

The aging central nervous system (CNS) is often marked by myelin degeneration, yet the underlying mechanisms remain elusive. This study delves into the previously unexplored role of autophagy in maintaining CNS myelin during aging. We generated the transgenic mouse line *plpCre^{ERT2}*; *atg5$^{f/f}$*, enabling selective deletion of the core autophagic component Atg5 in oligodendrocytes (OLs) following tamoxifen administration in adulthood, while analysis was conducted on aged mice. Our findings reveal that oligodendroglial autophagy inactivation leads to significant alterations in myelin protein levels. Moreover, the ultrastructural analysis revealed pronounced myelin deficits and increased degeneration of axons, accompanied by apoptosis, as confirmed by immunohistochemistry. Behaviorally, aged knockout (cKO) mice exhibited marked deficits in learning and memory tasks, indicative of cognitive impairment. Additionally, we observed increased activation of microglia, suggesting an inflammatory response linked to the absence of autophagic activity in OLs. These results underscore the critical role of autophagy in OLs for the preservation of CNS myelin and axonal integrity during aging. Our study highlights autophagy as a vital mechanism for neural maintenance, offering potential therapeutic avenues for combating age-related neurodegenerative diseases.

1 | Introduction

Central nervous system (CNS) myelin, a critical component for the efficient transmission of nerve impulses, undergoes significant changes during the aging process. Myelin is a lipid-rich membrane produced by oligodendrocytes (OLs) that insulates the axons, provides metabolic support, and ensures the rapid action potential propagation and precise communication within the brain and spinal cord. Indications of myelin abnormalities are evident in various neurodevelopmental disorders (de Faria Jr. et al. 2021; Galvez-Contreras et al. 2020; Stedehouder and Kushner 2017; Xekardaki et al. 2011), as well as in conditions linked to adulthood and aging, such as Alzheimer's disease (AD) (Bartzokis 2011; Dean et al. 2017; Depp et al. 2023; Mathys et al. 2019), Parkinson's disease (Dean et al. 2016; Rodriguez-Diehl et al. 2019; Yang et al. 2023), Huntington's disease (Bartzokis et al. 2007; Casella et al. 2020) and amyotrophic lateral sclerosis (ALS)

(Kang et al. 2013). In fact, recent findings reveal that myelin breakdown is a crucial early event in AD, exacerbating its progression (Depp et al. 2023).

Notably, even in normal aging, magnetic resonance imaging (MRI) has revealed a range of alterations in white matter in aging brains (Bartzokis et al. 2003, 2010; Salat et al. 2005). Additionally, specific myelin irregularities have been identified in postmortem tissue from aged humans and other primates (Lintl and Braak 1983; Marner et al. 2003; Peters 2002; Tang et al. 1997), as well as rodents (Safaiyan et al. 2016). Electron microscopy studies on aged rodents and non-human primates have shown that the most significant changes during the aging process primarily involve alterations in the structure of myelinated nerve fibers, characterized by myelin decompaction and splits in the intraperiod and major dense lines (Peters 2002; Safaiyan et al. 2016). Recently, multiphoton live imaging of the upper cortical layers in mice has corroborated these findings, revealing myelin degeneration and the loss of internodes with advancing age (Hill et al. 2018). Namely, as age progresses, a notable proportion of myelin sheaths exhibit degenerative transformations, leading to a decline in cognitive and motor functions (Bartzokis 2004). This degeneration is often linked to an imbalance in the maintenance and repair mechanisms of myelin, which become less efficient over time. Microglia are known to participate in these mechanisms by specifically phagocytosing myelin sheaths (Hughes and Appel 2020; Djannatian et al. 2023; Safaiyan et al. 2016). However, it was not until very recently that macroautophagy in OLs was proposed as a cell-autonomous mechanism for myelin degradation by our group and others (Ktena et al. 2022; Aber et al. 2022). When autophagy is ablated specifically in OLs in adulthood, PLP accumulation, myelin decompaction, increased axonal degeneration, and behavioral deficits are evident (Ktena et al. 2022).

Autophagy represents a housekeeping process responsible for the degradation and recycling of various components within the brain, such as misfolded protein aggregates, damaged or superfluous mitochondria, and endoplasmic reticulum, as well as myelin-related and synaptic proteins through the lysosomal machinery (Kallergi et al. 2023). Recent studies have linked impairment of general autophagy or subtypes of autophagy with a plethora of neurodegenerative diseases, as well as CNS myelin disorders, representing a significant factor contributing to these diseases and holding potential as a therapeutic target (reviewed in Menzies et al. 2017; Nutma et al. 2021). During aging, the prevailing view—led mainly by studies in invertebrate models—was that brain autophagy declines (reviewed in Aman et al. 2021). However, research presents conflicting evidence regarding whether brain autophagy diminishes with normal aging in mammals, and the most recent data have pointed to the observation that the autophagic degradome is relatively stable between the adult and aged brain (Kallergi and Nikoletopoulou 2021; Kallergi et al. 2023). Similarly, mitophagy was found to also be stable or even increase in certain brain areas with aging (Jimenez-Loygorri et al. 2024). Understanding the mechanisms that regulate autophagy in OLs in the aging CNS could provide valuable insights into potential therapeutic strategies aimed at preserving myelin integrity and mitigating age-related cognitive decline.

In the last decade, a limited number of publications mostly focused on the role autophagy plays in OLs and CNS myelin after trauma (Saraswat Ohri et al. 2018; Munoz-Galdeano et al. 2018) but also under steady-state conditions during myelin development and in adulthood (Bankston et al. 2019; Aber et al. 2022; Ktena et al. 2022). However, the role of this pathway in CNS myelin specifically during aging has never been assessed before. The aim of this study is to elucidate the role of autophagy in myelin homeostasis in the aged CNS. Our findings strongly support that autophagy is an essential mechanism for myelin maintenance and neuronal survival during aging. We demonstrate that autophagy depletion in OLs in vivo leads to alterations in the myelin protein levels and significant morphological defects in the myelin membrane, accompanied by increased axonal degeneration and apoptosis. As a result, aged mice exhibit behavioral deficits. Altogether, these findings show that selective disruption of autophagy in OLs is sufficient to alter CNS myelin homeostasis in the aged brain, leading to neurodegeneration and inducing defects in behavior.

2 | Materials and Methods

2.1 | Mouse Lines

The animal protocols for this study were approved by the Animal Ethics Committee of the Foundation for Research and Technology Hellas (FORTH). All animals were maintained under temperature-controlled conditions on a 12-h light/dark cycle, with a standard chow diet and water available ad libitum in the animal facility of the Institute of Molecular Biology and Biotechnology (IMBB)—FORTH (license numbers: EL91-BIObr-01 and EL91-BIOexp-02). All experiments adhered to ARRIVE and NC3Rs guidelines to enhance laboratory animal welfare and complied with regulations and standards outlined in Presidential Decree 56/30.04.2013 (Greek Law), in alignment with EU directives (2010/63/EU and L 276/33/20.10.2010) and the UK Animals (Scientific Procedures) Act, 1986, equivalent to NIH standards. Both male and female mice were included in this study in behavioral and immunohistochemistry experiments, since no sex differences were detected in these assays ($n_{\text{control-males}} = 13$ mice, $n_{\text{cKO-males}} = 10$ mice, $n_{\text{control-females}} = 5$ mice, $n_{\text{cKO-females}} = 4$ mice). *Plp-Cre*^{ERT2}; *atg5*$^{f/f}$ mice were obtained by crossing the *atg5*$^{f/f}$ mice (Hara et al. 2006, kindly provided by Dr. Chamilos, Heraklion) with *plpCre*^{ERT2} (Leone et al. 2003, kindly provided by Dr. Suter, Zurich). For in vivo gene KO induction, tamoxifen (Sigma-Aldrich, Cat# T5648), dissolved in a sunflower oil/ethanol (9:1) mixture at a concentration of 10 mg/mL, was administered via intraperitoneal injections at a dose of 1 mg/mouse/day for 10 days with a two-day break in between, as previously described (Leone et al. 2003) starting at 2.5 months. Mice of both genotypes were treated with tamoxifen. The mice were sacrificed at 22–24 months (for simplicity referred to as 22 months).

2.2 | Immunohistochemistry

For immunohistochemistry, brains were collected following transcardiac perfusion with 4% paraformaldehyde (PFA) in 0.1 M phosphate-buffered saline (PBS). The tissues were

post-fixed in the same fixative for 30 min at 4°C, then cryoprotected overnight in 30% sucrose in 0.1 M PBS and embedded in a 7.5% gelatin/15% sucrose gel. Optic nerve samples were not embedded in gelatin/sucrose gels but were immediately sectioned in the cryostat. Sections with a thickness of 10 μm for optic nerves and 15 μm for brains were collected on Superfrost Plus microscope slides (O. Kindler), post-fixed in ice-cold acetone for 10 min, blocked in 5% BSA (Sigma-Aldrich) in 0.1 M PBS for 1 h at room temperature, and incubated with primary antibodies overnight at 4°C, followed by secondary antibodies for 2 h at room temperature, both in 5% BSA and 0.5% Triton-X in 0.1 M PBS.

We have analyzed (a) different white matter tracts (corpus callosum, optic nerves) to assess myelin and axonal integrity as well as OL populations and (b) gray matter areas (hippocampus). The hippocampus was chosen to assess OL populations, microglia, and apoptosis, due to the behavioral defects observed in the aged animals.

The following primary antibodies were used: anti-MBP (1:200, rat, Serotec Cat# MCA409S), anti-adenomatous polyposis coli clone CC1 (APC/CC-1) (1:100, mouse, Millipore Cat# OP80) anti-platelet derived growth factor receptor alpha (PDGFRa) (1:100, rat, Millipore Cat# CBL1366), anti-MAP2 (1:400, mouse, Merck, Cat# MAB3418), anti-NeuN (1:1000; rabbit, Cell Signaling, Cat#24037), anti-IBA-1 (1:500; rabbit, Invitrogen, Cat# PA5-21274), anti-CD11b (1:100; rat, BD-Biosciences, Cat# 553311), anti-Caspase 3, active (cleaved) form (1:400; rabbit, Cell Signaling, Cat# 9661).

Fluorochrome-labeled secondary antibodies Alexa Fluor 555 (1:800, anti-mouse, ThermoFisher, Cat# A-21422), CF488 (1:800, anti-rabbit, Biotium, Cat# 20012), CF488A (1:800, anti-rat, Biotium, Cat# 20023), and Cy3 (1:800, anti-rabbit, Jackson ImmunoResearch, Cat# 111-165-003) were also used. DAPI (1:2000, Invitrogen, Cat# MP01306, USA) was finally used for the visualization of the nuclei.

2.3 | Electron Microscopy

2.3.1 | Tissue Preparation

For electron microscopy, mice were perfused with 2.5% glutaraldehyde in 0.1 M phosphate buffer (PB), pH 7.25. The dissected optic nerves were placed in the primary fixative overnight at 4°C, and sample preparation followed the method of Pasquettaz et al. (2021). Briefly, samples were extensively washed in 0.1 M PB, then incubated in 2% (wt/vol) osmium tetroxide and 1.5% (wt/vol) K4[Fe(CN)6] in 100 mM PB buffer for 1 h on ice. After thorough washing with water, samples were incubated for 1 h in 1% (wt/vol) tannic acid in 100 mM PB buffer, followed by 2 h in 1% (wt/vol) uranyl acetate at room temperature. The samples were then dehydrated at room temperature in gradual ethanol cycles and infiltrated with a mix of ethanol and Epon-Araldite (EMS). After multiple cycles of 100% Epon-Araldite incubations, samples were flat embedded and polymerized for 24 h at 60°C (Kolotuev 2014). Control and cKO samples were processed simultaneously to avoid artifacts from fixation or embedding.

2.3.2 | Transmission Electron Microscopy (TEM)

Polymerized flat blocks were trimmed using a 90° diamond trim tool (Diatome, Biel, Switzerland). Arrays of 70 nm sections were obtained using a 35° diamond knife (Diatome, Biel, Switzerland) mounted on a Leica UC6 microtome (Leica, Vienna). The optic nerves were oriented perpendicular to their length for cross-sections approximately 1 mm from the optic nerve head. Sections were collected on polyetherimide-coated carbon slot grids.

TEM samples were analyzed with an FEI CM100 electron microscope (Thermo Fisher Scientific) at 80 kV, equipped with a TVIPS camera, controlled by the EMTVIPS program. Images were collected either as single frames or stitched mosaic panels to cover extensive sample regions. Multiple tile images were stitched using the IMOD software package (Kremer et al. 1996). Data were processed and analyzed using Fiji, IMOD 3dmod, and Photoshop programs.

2.4 | Western Blot Analysis

Tissues were collected and stored at −80°C until homogenization. The number of animals for each experiment is indicated in the results section. Briefly, tissues were lysed by sonication in RIPA buffer (50 mM Tris–HCl pH 8.0, 150 mM NaCl, 1% Triton X-100, 0.5% sodium deoxycholate [DOC]) supplemented with a protease inhibitor cocktail (Sigma-Aldrich, Cat# P8340), incubated on ice for 20 min, and centrifuged at 18,000 *g* for 20 min. Protein samples were separated on 12% polyacrylamide gels and transferred to nitrocellulose membranes (Millipore) for 1 h at 310 mA. After blocking in 5% BSA (Sigma-Aldrich) for 1 h at room temperature, membranes were incubated with primary antibodies overnight at 4°C. The following antibodies were used for Western blot (WB) analysis: anti-PLP (1:1000, rabbit, Abcam Cat# ab28486), anti-MBP (1:2000, rat, Serotec Cat# MCA409S), anti-Atg5 (1:1000; rabbit, Novus, Cat# NB110-53818), anti-CNPase (1:1000; rabbit, Cell Signaling, Cat# 5664), and anti-α-Tubulin, clone DM1A (1:10,000; mouse, Sigma-Aldrich, Cat# T9026). After three 5-min washes in TPBS (100 mM Na2HPO4, 100 mM NaH2PO4, 0.5 N NaCl, 0.1% Tween-20), membranes were incubated with secondary horseradish peroxidase-conjugated antibodies (Millipore, Cat# AP308P, AP132P, AP189P) for 1 h at room temperature. Blots were developed using the Immobilon Classico Western HRP substrate (Merck, Cat# WBLUC0500) per the manufacturer's instructions. Quantification of band intensity was performed using the Fiji/ImageJ Gel Analyzer plugin.

2.5 | Real-Time PCR

Total RNA was extracted from optic nerve samples of control and cKO animals (three animals per group) using the RNAiso-plus kit (Takara) following the manufacturer's instructions. cDNA synthesis was performed through reverse transcription from the total RNA using the PrimeScript first strand cDNA synthesis kit (Takara, Cat. #6110A). Gene expression levels of plp (forward primer: 5′-TCAGTCTATTGCCTTCCCTA-3′, reverse primer: 5′-AGCATTCCATGGGAGAACAC-3′), mbp (Pernet et al. 2008, forward primer: 5′-CACACACGAGAACTACCCA-3′, reverse primer: 5′-GGTGTTCGAGGTGTCACAA-3′) and

2′.3′-Cyclic-nucleotide 3′-phosphodiesterase (cnp) (Pernet et al. 2008, forward primer: 5′-AGGAGAAGCTTGAGCTGGTC-3′, reverse primer: 5′-CGATCTCTTCACCACCTCCT-3′) were assessed by real-time PCR using a StepOnePlus real-time PCR system (Applied Biosystems, Life Technologies, Thermo Fisher Scientific Inc., Waltham, MA). Gapdh was used as the internal control (forward primer: 5′-ATTGTCAGCAATGCATCCTG-3′, reverse primer: 5′-ATGGACTGTGGTCATGAGCC-3′). Each sample's PCR runs were performed in triplicates, and the expression levels for each gene were normalized to the internal control.

2.6 | Behavior

2.6.1 | Open Field Test (OFT)

After completing the initial handling procedures, the locomotor activity and anxiety levels of the mice were assessed. The mice were introduced to the experimental room 1 h prior to the test for acclimation. Each mouse was placed in the center of an open field arena measuring 45 × 45 × 45 cm and allowed to move freely for 10 min. Their activity was recorded on video throughout the task. The arena was cleaned with 70% ethanol between each test subject. Anxiety was assessed by measuring the percentage of time spent in the center zone. Locomotion was assessed by tracking each animal's path and calculating the total distance traveled. The video recordings were analyzed using software tools such as JWatcher and ANY-maze. The results were based on each subject's activity during the first 5 min of the test.

2.6.2 | Object Recognition Tests

Object exploration was defined as the time spent interacting with the objects through activities like touching and sniffing. Preliminary trials confirmed that the mice did not exhibit a specific preference for any of these objects. Prior to the day of behavioral testing, all animals were habituated to the testing environment without any objects present for a duration of 10 min each day over three consecutive days. The time that mice explored the two different objects was measured, and the discrimination index was calculated. Mice with a total exploration time < 0.02% for both objects for either the training or testing phase were excluded from the analysis, as it cannot be confirmed they spent enough time exploring to learn/discriminate.

2.6.3 | Novel Object Recognition

The novel object recognition (NOR) memory task consisted of two phases, a sample trial and a test trial, with a 25-min interval in between. During the sample trial, two identical novel objects were placed in the open field, and the animals were allowed to explore for 10 min. In the subsequent test trial, the same two positions held one familiar object from the sample trial and one novel object unfamiliar to the mice. The duration of exploration for each object was recorded. After each trial, the objects and the open field were cleaned with a 70% ethanol solution to eliminate any odor cues. The discrimination index was calculated as the time of exploration of the novel object to the time of exploration of the familiar one, divided by the total investigation time for both objects.

2.6.4 | Object Location Recognition

The object location recognition memory task was conducted at least 2 days after the completion of the NOR. In the sample trial, the animals explored two identical copies of an object in the apparatus for 5 min. Following a 25-min interval, a 5-min test trial was administered, similar to the sample trial but with one object remaining in the same position (stationary) and the other moved to a new position (displaced). Object location recognition memory was defined by an increase in the time spent exploring the displaced object compared to the stationary one, according to the criteria of Dere et al. (2007) and Ennaceur and Aggleton (1997). The discrimination index was calculated as the time of exploration of the displaced object to the time of exploration of the stationary one, divided by the total investigation time for both objects.

2.6.5 | Temporal Object Recognition

Two days after completing the object location recognition task, the animals were subjected to the temporal order object recognition task. This task involved two sample trials followed by one test trial, with a 25-min interval between trials. In each sample trial, the animals explored two identical copies of the same object for 5 min. Different objects were used in each of the two sample trials. During the test trial, one object from the first sample trial (the older one) and one from the second sample trial (the more recent one) were presented, allowing the animals 5 min to explore the open field. The positions of the objects remained the same across both the sample trials and the test trial. Temporal order object recognition memory was defined by an increase in the time spent exploring the older familiar object compared to the more recent familiar object, based on the criteria established by Mitchell and Laiacona (1998). The discrimination index was calculated as the time of exploration of the old object to the time of exploration of the more recent one, divided by the total investigation time for both objects.

2.7 | Rotarod Test

Motor behavior in mice was assessed using a rotarod apparatus (MK-660D, Muromachi-Kikai, Tokyo, Japan). The training was conducted over five consecutive days, with four trials per day, separated by 15-min rests between trials. Every trial was video recorded. The mice were placed on the rotating rod at 4 rpm for the first 3 days, gradually increasing the speed to 40 rpm. On the fourth and fifth days, the task consisted of two consecutive sessions of three trials each, with a constant speed of 20 rpm for the first session and 32 rpm for the second session.

The test was conducted under low illumination conditions, and the device was wiped clean with 70% ethanol before placing subjects from a different cage on it. A trial was considered over when all mice had performed two rotations, when all mice had fallen off, or when the cutoff time was reached (i.e., 5 min). An

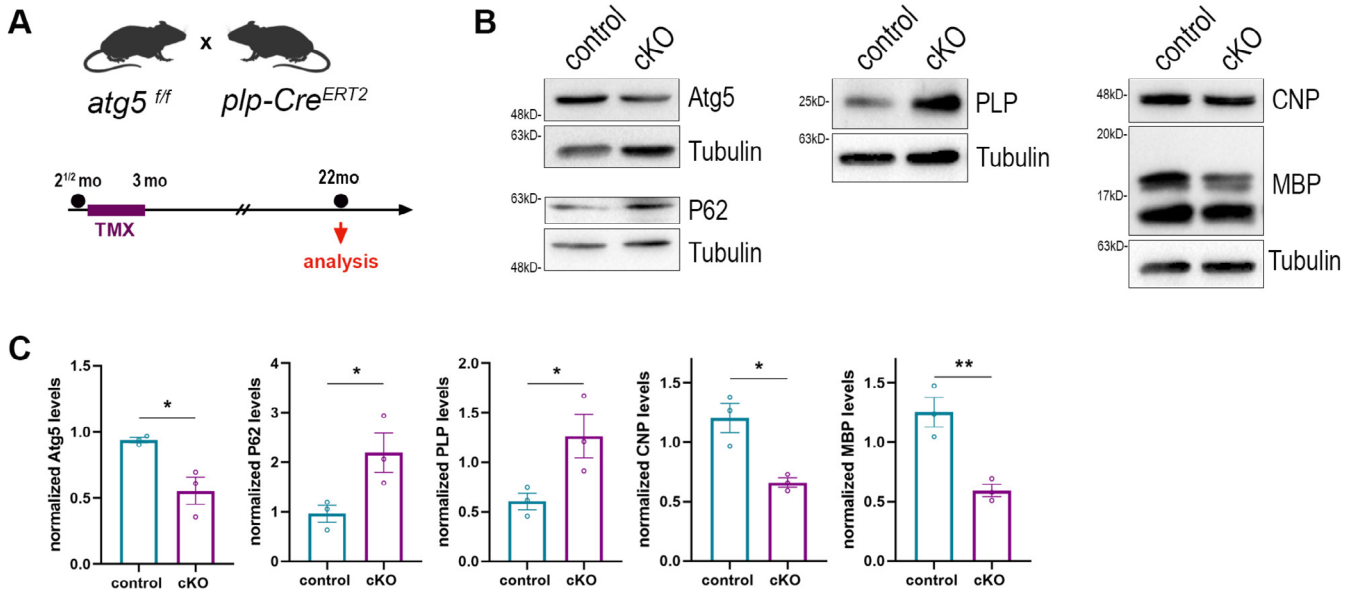

FIGURE 1 | Depletion of autophagy in oligodendrocytes leads to modulation of structural myelin proteins in aged mice. (A) Scheme illustrating the generation of *plp-Cre*^{ERT2}; *atg5*$^{f/f}$ mice and the experimental protocol used for tamoxifen (TMX) induction and analysis. TMX was injected intraperitoneally at a dose of 1 mg per day for 10 days with 2 days of break in between, starting at the age of 2.5 months in all mice. The analysis was performed at 22 months of age. (B) Western blot analysis of optic nerve lysates from 22-month-old control and cKO mice with antibodies against Atg5, P62, CNP, PLP, and MBP proteins. Representative images from a single experiment are shown. (C) Quantification of normalized protein levels as depicted in (B). Data information: Data are presented as mean ± SEM. $N = 3$ animals per genotype. Statistical significance was determined using an unpaired, two-tailed Student's *t*-test (*$p < 0.05$, **$p \leq 0.01$).

average of the four trials per day for each mouse was calculated. The duration each mouse stayed on the rod was recorded for analysis.

2.8 | Hindlimb Clasping Test

In addition to the rotarod test, which assessed the motor coordination of both male and female mice, we conducted the hindlimb clasping test on Day 5. This test serves as a marker for monitoring disease progression in mouse models of neurodegeneration and ataxia.

The experimental procedure involved gently lifting each mouse by the tail, ensuring it was clear of any nearby objects, and holding it in the air for a duration of 10 s. After each session, the mice were returned to their respective home cages. All sessions were recorded on video, and the mice were evaluated based on their hindlimb motor behavior. Specifically, mice that consistently extended their hindlimbs outward from their abdomen, showing normal escape tension, were assigned a score of 0. A score of 1 was given to mice that retracted one hindlimb toward the abdomen for more than 5 s. If both hindlimbs were partially retracted for more than 50% of the time, a score of 2 was assigned. Finally, mice that fully retracted both hindlimbs for more than 5 s received a score of 3.

2.9 | Statistical Analysis

In all experiments, data were expressed as mean ± SEM. For normally distributed values, parametric tests, including two-tailed unpaired *t*-test and one-way analysis of variance (ANOVA) followed by Tukey post hoc test for multiple comparisons, were used. For non-normally distributed values, non-parametric tests such as the Mann–Whitney test or Kruskal–Wallis test with Dunn's post hoc tests for multiple comparisons were employed. Statistical analysis was conducted using GraphPad Prism 8 software (GraphPad Software, San Diego, CA). *p* values < 0.05 were considered statistically significant.

3 | Results

3.1 | Inactivation of Oligodendroglial Autophagy Leads to Alterations in Myelin Protein Levels in Aged Mice

To investigate the role of autophagy in OLs in CNS myelin in aging in vivo, we crossed *atg5*$^{f/f}$ mice with tamoxifen-inducible *plpCre*^{ERT2} mice. This allowed us to selectively eliminate the core autophagic component Atg5 in myelinating glial cells following tamoxifen administration. The successful recombination exclusively in myelinating glial cells—and therefore myelin tracts—has been previously verified and described, using the *mT/mG* transgenic reporter mouse line (Ktena et al. 2022). In our experimental protocol, we administered tamoxifen to *plp-Cre*^{ERT2}; *atg5*$^{f/f}$ mice at 2.5 months of age using the protocol previously described (Ktena et al. 2022) and analyzed both control (*atg5*$^{f/f}$) and cKO (*plpCre*^{ERT2}+; *atg5*$^{f/f}$) animals at 22–24 months of age (for simplicity referred to as 22 months) a timepoint that is considered as "aging" that has not been evaluated before (Figure 1A). Mice of both genotypes were treated with tamoxifen, as explained in the Section 2.

Recent research has established that new myelin-forming OLs are generated in the mouse CNS during adulthood (Tripathi et al. 2017). Given that recombination induction and autophagy ablation occurred at 2.5 months of age and the analysis was conducted at 22–24 months, we first confirmed that autophagic activity was decreased in the aged cKO mice. Western blot analysis confirmed the reduction of autophagy in aged cKO mice by showing decreased levels of the Atg5–Atg12 complex of 55 kD by about 50%, and at the same time increased levels of the autophagic receptor P62, compared to age-matched controls (Figure 1B,C).

Our primary objective was to assess whether key protein constituents of myelin, specifically PLP, MBP, and CNP, were altered in the mutants. PLP protein levels were found to be increased in the Western blot analysis of 22 months cKO mice, whereas MBP and CNP levels were decreased (Figure 1B,C). Unlike the optic nerve data, extracts from the cerebral cortex do not show differences in PLP/MBP expression levels in aged control and cKO (Figure S1 and Section 4). To determine if the changes in myelin protein expression in aged cKO mice were due to transcriptional dysregulation of myelin genes following autophagy ablation, we performed quantitative real-time PCR on optic nerve extracts from aged control and cKO animals to measure the mRNA levels of the *plp*, *mbp*, and *cnp* genes (Figure S2A). The mRNA levels of these genes were unchanged between aged control and cKO optic nerves, suggesting that autophagy directly affects myelin protein levels rather than their gene transcription levels.

3.2 | Autophagy in OLs Is Crucial for Maintaining CNS Myelin and Axonal Integrity in Aging

We then examined whether autophagy ablation affects myelin integrity and axonal maintenance by performing electron microscopic (EM) analysis of 22 months control and cKO optic nerves (Figure 2). This analysis revealed increased numbers of axons with decompacted myelin and significantly increased axonal degeneration in mutant mice (Figure 2A,B). Additionally, axon diameter analysis showed a small but statistically significant redistribution of axon caliber diameters, with 22 months cKO axons exhibiting a loss of large caliber axons (Figure 2C). G-ratio analysis, which consists of a measurement of myelin sheath thickness, indicated that autophagy-deficient axons had extended myelin sheaths (smaller g-ratio) compared to controls (Figure 2D). We consider that this extension reflects the loosening of myelin lamellae, which will finally lead to the increased myelin decompaction. These results suggest that large caliber axons are particularly vulnerable to autophagic dysfunction. In our recent work (Ktena et al. 2022), we noticed similar deficits in myelin integrity; however, these are exacerbated in all three types of assessment when the same genetic model is analyzed at 22 months of age (Figure S3).

3.3 | The Depletion of Oligodendroglial Autophagy Leads to Memory Deficits in Aged Mice, While Motor Ability Remains Unaltered

Our findings prompted us to investigate whether the disruption of autophagy in OLs leads to functional impairments during aging. We examined behaviors related to memory, motor learning, and motor coordination. Traditionally, oligodendroglial cells were thought to have little association with synaptic plasticity in learning. However, recent evidence from human and animal studies suggests that oligodendroglia play a role in various forms of learning and memory (McKenzie et al. 2014; Pan et al. 2020; Steadman et al. 2020). To this direction, we performed three different types of object-recognition assays in aged control and cKO mice: (1) novel object recognition, (2) object location recognition, and (3) temporal-order object recognition tasks (Figure 3).

In the novel object-recognition task, aged cKO mice had a significantly reduced discrimination index compared to age-matched controls. In the object-location and temporal-order recognition tasks, aged cKO mice showed a discrimination index similar to aged controls, although in the object-location task, control mice had a tendency to spend more time exploring the displaced object over the stationary one, compared to cKOs.

We also investigated whether autophagy depletion affects anxiety-like states by evaluating the time spent in the center of an open field, which is inversely associated with anxiety (Figure S4A). No significant differences were found between the groups. Additionally, no significant change was observed in the total distance traveled, excluding locomotor alterations as a factor in our results (Figure S4A).

Moreover, to test motor learning and coordination, mice performed an accelerating rotarod test for three consecutive days (Costa et al. 2004). Both 22months control and cKO mice showed continuous improvement in performance over time during the 3-day trial, meaning they significantly improved their performance over time (Figure S4B). In the subsequent motor coordination phase, where latency to fall from a rod rotating at constant speeds of 20 and 32 rpm was tested, no differences were observed between the groups in either speed (Figure S4C). Consistent with these findings, the clasping test also showed no significant impact on motor coordination (Figure S4D).

In summary, no differences were observed in anxiety-like states, motor coordination, or motor learning between control and age-matched cKO animals. In contrast, when tested in memory and learning assays, aged cKO mice showed lower performance in the novel object-recognition test and a tendency for lower performance in the temporal-order recognition test, while they performed similarly to control mice in the object-location recognition test.

3.4 | Autophagic Depletion in OLs Leads to Neuronal Apoptosis

The ultrastructural results, which revealed increased neurodegeneration in the axons of cKO mice, led us to hypothesize that neuronal death might be occurring as a consequence of autophagic ablation in OLs. To investigate this hypothesis further, we performed immunohistochemical analysis, staining with antibodies recognizing activated caspase-3 (casp3), a known apoptotic marker, in the hippocampus of control and cKO mice. The reason we focused on the hippocampus, rather than another brain region, was due to the deficits observed in object recognition tasks described above, which are known to be hippocampal-dependent (Clark et al. 2000).

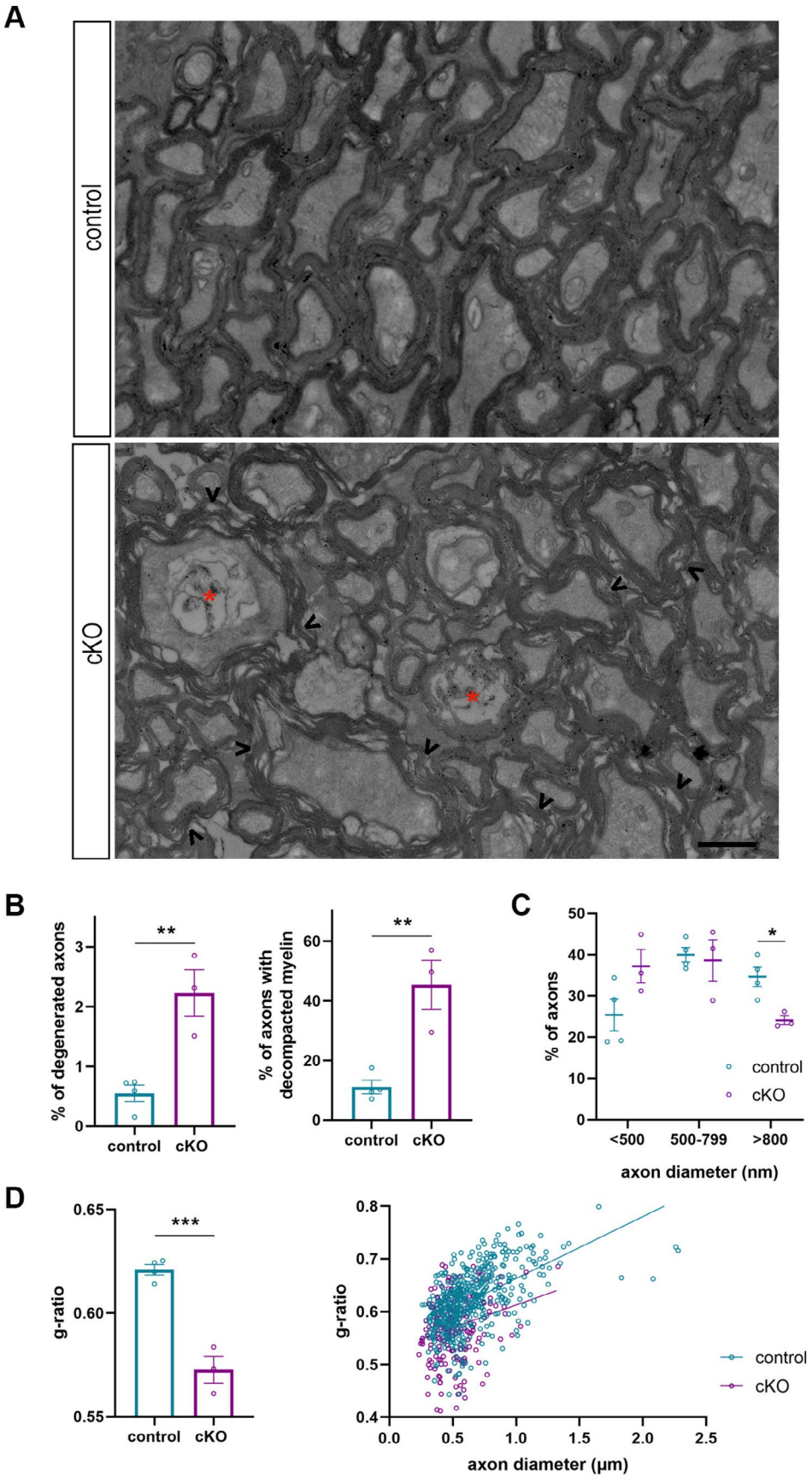

FIGURE 2 | Legend on next page.

FIGURE 2 | Autophagy in OLs is crucial for the maintenance of CNS myelin during aging. (A) Ultrastructural analysis of optic nerves from 22 months *plpCre*^{ERT2}-; *atg5*$^{f/f}$ (control) and *plpCre*^{ERT2}+; *atg5*$^{f/f}$ (cKO) mice. Representative electron micrographs of cross sections of control and cKO optic nerves, highlighting degenerating axons (red stars) and decompacted myelin sheaths (arrowheads). (B) Quantification of axonal degeneration and decompacted myelin sheaths in control and cKO mice (600–800 axons measured per mouse, student's *t*-test). (C) Quantification of the percentage of axons with small (< 500 nm), medium (500–799 nm), and large (> 800 nm) caliber in control and cKO optic nerves (300–360 axons measured per mouse, student's *t*-test). (D) Assessment of myelin sheath thickness using the g-ratio measurement from EM images of control and cKO animals. The plots display g-ratio values per animal group, with each point representing an animal, and g-ratio distribution for different axonal diameters in both groups, with each point representing an axon (linear regression, 468 axons for control, 220 axons for the cKO group). Scale bar: 1 μm. Data information: Data are presented as mean ± SEM. $N = 3–4$ animals per genotype. Statistical significance was determined using an unpaired, two-tailed Student's *t*-test. (*$p < 0.05$, **$p \leq 0.01$, ***$p \leq 0.001$).

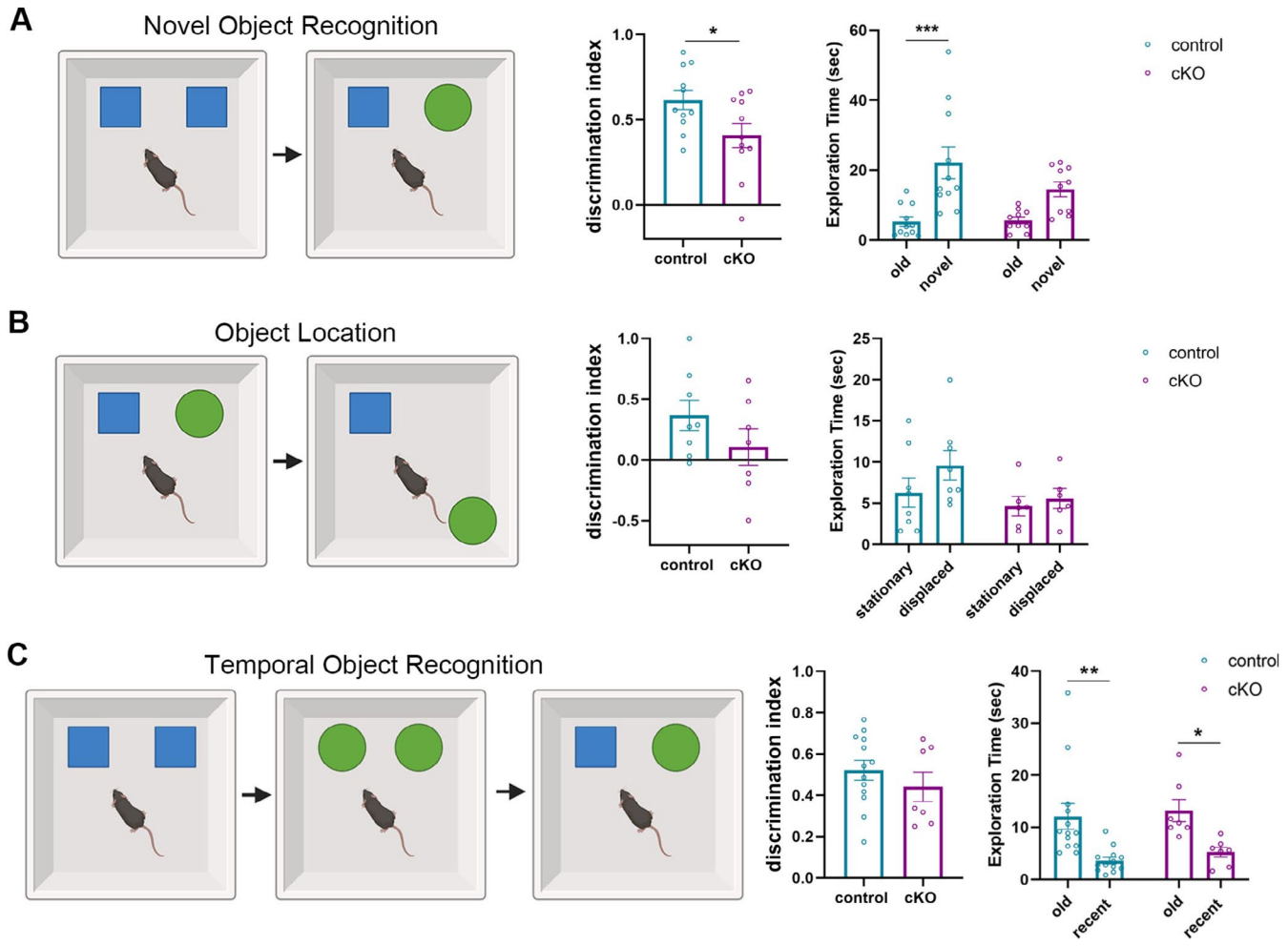

FIGURE 3 | Animals with autophagy deficiency in oligodendrocytes exhibit deficits in the novel object recognition task. (A) Schematic of the experimental setup for the novel object recognition test (NOR). The discrimination index is measured as the percentage of time spent observing the novel object minus the time spent observing the familiar object, divided by the total investigation time for both objects ($n_{control} = 11$ mice, $n_{cKO} = 10$ mice; unpaired *t*-test $p = 0.0334$). For exploration time, Sidak's multiple comparisons test was used ($p_{control} = 0.0001$; $p_{cKO} = 0.0575$). Mice with total exploration time < 0.02% were excluded from analysis. (B) Schematic of the experimental setup for the object location test. The discrimination index is measured as the percentage of time spent observing the displaced object minus the time spent observing the stationary object, divided by the total investigation time for both objects ($n_{control} = 8$ mice, $n_{cKO} = 7$ mice; unpaired *t*-test $p = 0.2029$). For exploration time Sidak's multiple comparisons test was used ($p_{control} = 0.2516$; $p_{cKO} = 0.9153$). Mice with total exploration time < 0.02% were excluded from analysis. (C) Schematic of the experimental setup for the temporal object recognition test. The discrimination index is measured as the percentage of time spent observing the old familiar object minus the time spent observing the new familiar object, divided by the total investigation time for both objects ($n_{control} = 13$ mice, $n_{cKO} = 7$ mice; unpaired *t*-test $p = 0.3502$). Mice with total exploration time < 0.02% were excluded from analysis. Sidak's multiple comparisons test was used ($p_{control} = 0.0015$; $p_{cKO} = 0.0309$). Data information: Bars represent mean ± SEM. Student's *t*-test (for discrimination index) and Two-way ANOVA (Sidak's multiple comparisons test, for exploration time comparisons) were used to determine statistical significance. *$p < 0.05$, **$p < 0.01$, ***$p < 0.001$.

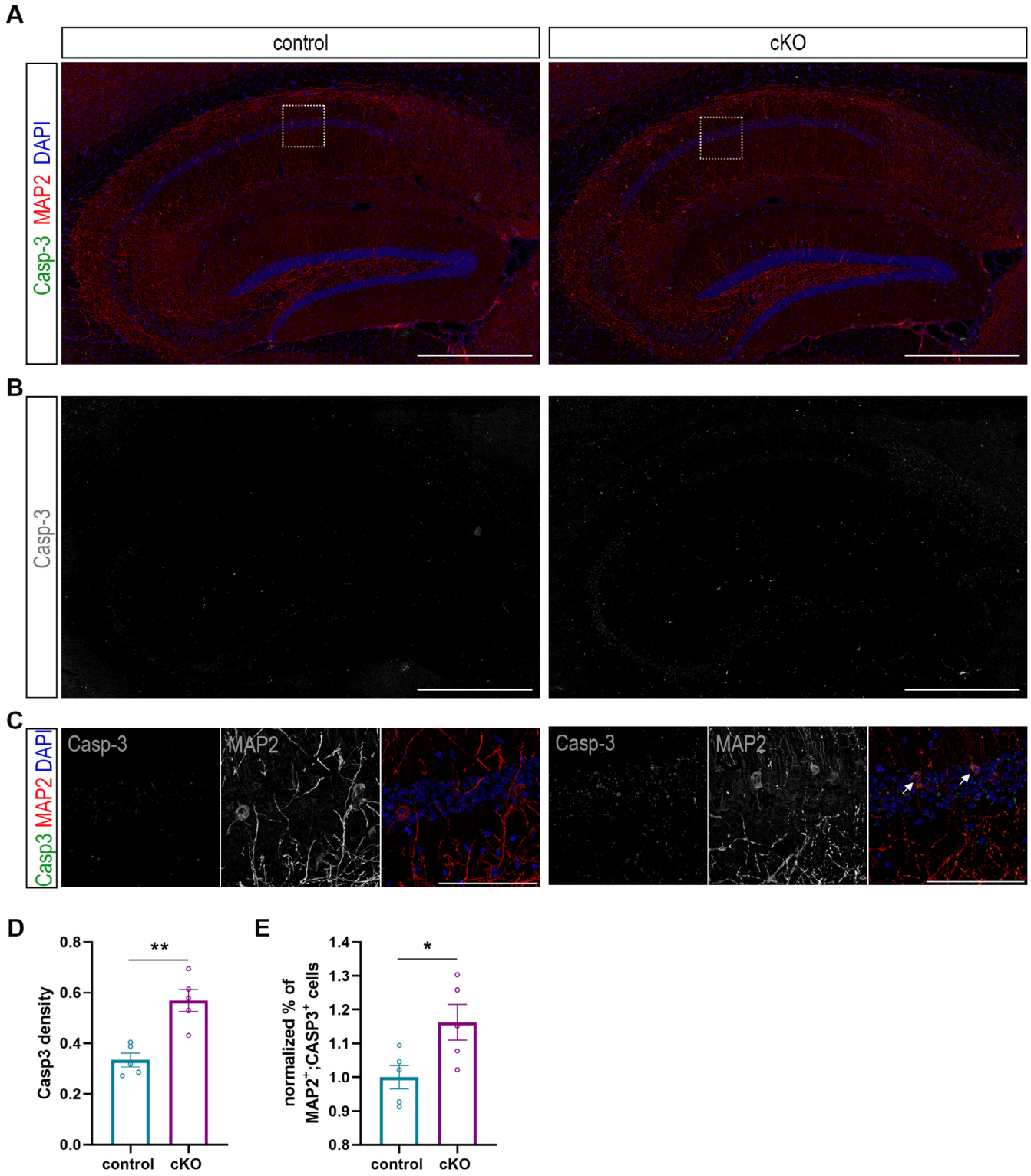

FIGURE 4 | Depletion of autophagy in OLs results in increased apoptosis. (A) Representative confocal images of hippocampal cryosections from 22-month-old transgenic and control mice, immunostained for cleaved casp3 (green), MAP2 (red), and DAPI (blue). Areas indicated by rectangular boxes are magnified in (C). (B) The Casp3 channel is shown. (D) Quantification of casp3+ density in the hippocampus. (E) Quantification of MAP2+/Casp3+ cells in the hippocampus. Data information: Bars represent mean ± SEM. $N = 5$ animals per genotype; statistical significance was determined using Student's *t*-test. *$p \leq 0.05$, **$p < 0.01$. Scale bars: 500 μm (A and B), 100 μm (C).

Our immunohistochemical analysis showed a substantial increase in caspase-3 positive (casp3+) cells in the hippocampus of cKO mice compared to controls (Figure 4A,B,D), indicating elevated levels of apoptosis. This prompted us to delve deeper into the cellular consequences of autophagic ablation. The TEM analysis provided compelling evidence of increased neurodegeneration; thus, in order to confirm that the dying cells were neurons, we conducted co-staining for casp3 and

microtubule-associated protein 2 (MAP2), used as a neuronal marker (Figure 4C). The co-localization of casp3 and MAP2 in the hippocampal neurons of cKO mice demonstrated that the apoptotic cells were MAP2-positive (Figure 4D). However, quantification of the total number of neurons with NeuN did not show a statistical difference (Figure S5). This could be explained by the small number of MAP2-positive cells showing an apoptotic signal compared to the entire $NeuN^+$ hippocampal population. In addition, the caspase signal could reflect cells committed to apoptosis but not yet dead. Together, these results suggest that the ablation of autophagy in OLs increases neuronal apoptosis.

3.5 | Depletion of Autophagy Increases Microglia Density Without Affecting OL Numbers

We subsequently investigated the impact of prolonged autophagic ablation on OL populations. We conducted immunohistochemistry analysis against CC1 (mature OLs) and PDGFRα (oligodendrocyte precursor cells, OPCs) in different white matter tracts (coronal sections of the rostral corpus callosum (cc) and optic nerves) of 22 months control and cKO mice (Figures 5A and S6). No differences were observed in the numbers of the different subpopulations between the two groups (Figures 5B and S6). To further validate this, we performed immunohistochemical analysis, staining with antibodies recognizing activated casp3 and CC1, where no differences were observed between control and cKO mice (Figure S7). These results suggest that the loss of autophagy in mature OLs does not lead to differences in their numbers, even 18–20 months after autophagic ablation.

In our cKO mice, we observed a significant increase in axonal degeneration and defective myelin accumulation. According to the literature, microglia are the primary cells responsible for phagocytosing degenerated axons and clearing myelin debris (Djannatian et al. 2023; Hughes and Appel 2020). This is crucial for maintaining neural health and function, as microglia play a key role in CNS homeostasis. We therefore sought to examine the microglia density in the context of autophagic depletion in OLs. Toward this direction, we immunolabeled against the microglia-specific marker IBA1 in coronal sections of the rostral cc of 22 months control and cKO mice (Figure 5C). Increased microglia density was detected in the case of autophagic ablation (Figure 5D). To further validate this result, we also stained for CD11b (Figure 5E), the β-integrin marker of microglia (Roy et al. 2006). Anti-CD11b staining shows elevated CD11b density in the cc region of cKO mice, while lower CD11b density is observed in the microglia of control ones (Figure 5F). This alteration in microglia morphology may propose that microglia are activated in the case of autophagic ablation in OLs and suggest that autophagy in OLs and microgliosis might compensate for each other in myelin degradation and clearance during aging (Figure 5D).

4 | Discussion

In this study, we investigated the role of autophagy in OLs in CNS myelin homeostasis during aging and showed that this pathway represents an essential mechanism for CNS myelin maintenance since its ablation results in myelin defects, neurodegeneration, and behavioral deficits in aged mice.

Aging is a gradual process characterized by the progressive decline of physiological cellular pathways, leading to the diminution of physical and cognitive abilities. Multiple studies have shown that changes in nerve fibers and their myelin sheaths, which are believed to be influenced by aging, play a crucial role in age-related cognitive decline in both humans and other mammals. Notably, evidence suggests that even within the realm of normal aging, myelin irregularities are an early pathological sign appearing in OLs before degenerative markers emerge in neuronal populations (Peters 2002, 2009). Furthermore, distinct myelin structural abnormalities have been identified in postmortem tissue samples from elderly humans and other primates (Marner et al. 2003; Peters 2002; Tang et al. 1997), as well as in rodent models (Safaiyan et al. 2016).

In parallel, studies involving genetic analyses, pharmacological interventions, and longevity assessments in various animal models have clearly established a link between impaired autophagy and reduced health span, leading to a shorter lifespan (Pyo et al. 2013). Additionally, it is known that autophagy may be affected in a range of neurodegenerative diseases (Menzies et al. 2017). Our previous work (Ktena et al. 2022) points to the requirement of autophagy in OLs for axonal integrity and myelin maintenance in adulthood. To investigate the role that defective autophagy in OLs might play in myelin maintenance at aging, we employed a cKO line we had established (Ktena et al. 2022). In this line, the core autophagic gene *atg5* is ablated only in myelinating glia upon tamoxifen administration ($plpCre^{ERT2}$; $atg5^{f/f}$). The analysis was performed at 22 months of age, an age group widely considered as aging that has never been evaluated before.

At this age, ultrastructural analysis of optic nerves revealed several significant findings. Specifically, we noted a loss of large-caliber axons in aged cKO mice. Generally, higher axonal caliber leads to faster signal transmission through the nodes of Ranvier (Stassart et al. 2018). The specific loss of large-caliber axons is well-documented in neurodegenerative diseases, such as ALS, where neurons with large axon calibers are selectively affected (Hammad et al. 2007). Another plausible explanation for this phenomenon could be the brain's homeostatic response to the high energy cost of maintaining large-caliber axons (Perge et al. 2012). In parallel, our ultrastructural analysis showed a decrease in the g-ratio, as well as an increased presence of axons surrounded by decompacted myelin and degenerated axons. These important phenotypes are present in many demyelinating diseases, such as Pelizaeus-Merzbacher disease (PMD) (Anderson et al. 1998; Ip et al. 2006; Laukka et al. 2016). Additionally, the increased degeneration observed was also verified through immunohistochemistry, which revealed an elevated signal for cleaved casp3 in the region of the hippocampus, and specifically in the MAP2+ neurons. This increase is indicative of elevated apoptotic activity, aligning with the observed structural damage in the myelinated axons. The combination of TEM and immunohistochemistry provides robust evidence for the pronounced neurodegenerative effects present in our cKO model.

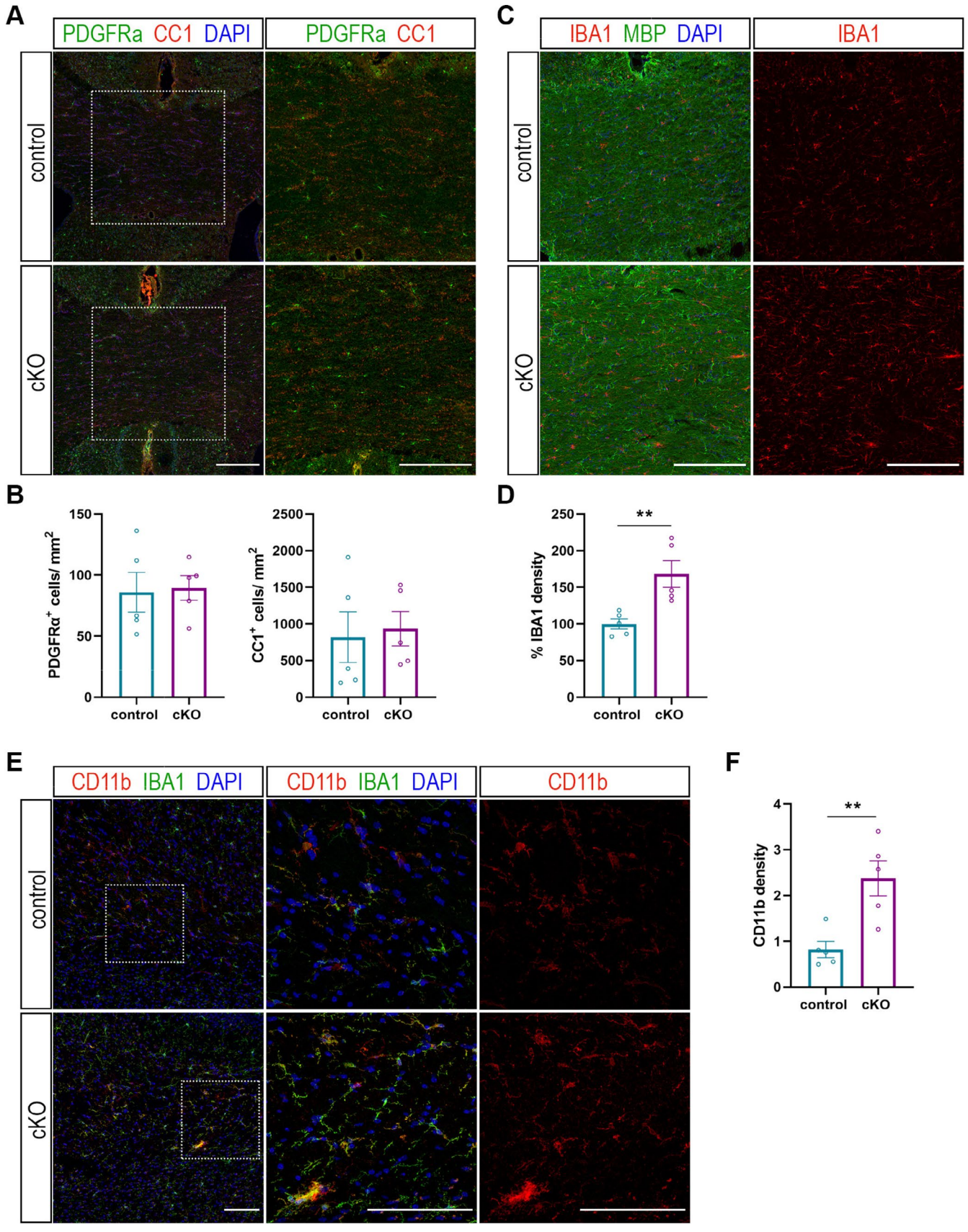

FIGURE 5 | Legend on next page.

FIGURE 5 | Depletion of autophagy increases microglia numbers, while OL populations remain constant. (A) Representative confocal images of rostral corpus callosum (cc) cryosections from 22-month-old transgenic and control mice, immunostained for PDGFRa (green), CC1 (red), and DAPI (blue). Areas indicated by rectangular boxes are magnified on the right. (B) Quantification of PDGFRa+ OPCs and CC1+ mature OLs in the cc. (C) Representative confocal images of rostral corpus callosum (cc) cryosections from 22-month-old transgenic and control mice, immunostained for IBA1 (red), MBP (green), and DAPI (blue). The IBA1 channel is shown in the right panel. (D) Quantification of IBA1+ microglia density in the cc. (E) Representative confocal images of corpus callosum (cc) cryosections from 22-month-old transgenic and control mice, immunostained for IBA1 (green), CD11b (red), and DAPI (blue). Areas indicated by rectangular boxes are magnified on the right, and the CD11b channel is shown. (F) Quantification of CD11b+ microglia density in the cc. Data information: Bars represent mean ± SEM. $N = 5$ animals per genotype; statistical significance was determined using Student's *t*-test. $^{**}p \leq 0.01$. Scale bars: 200 μm (A–C), 100 μm (E).

Myelin defects observed in aged mice overall are reminiscent of PMD, and this also came in accordance with the biochemical underpinnings. Specifically, Western blot analysis revealed a noticeable increase in the expression of proteolipid protein (PLP), in contrast to the reduced levels of MBP and CNP. We have previously shown that PLP protein is an autophagic cargo and that it is also maintained at high levels in young adult mice where autophagy is ablated specifically in OLs (Ktena et al. 2022). Notably, the observation of unaltered mRNA levels indicated that the observed phenotype is primarily due to changes in protein abundance rather than transcriptional modulation. The intricate interplay between myelin-associated proteins, including PLP, MBP, and CNP, presents a complex scenario where changes in the expression of one protein can affect others. In the PMD model, increased PLP affects the expression of other myelin protein levels, such as MBP and CNP, during myelination, leading to their reduction (Karim et al. 2007). MBP and CNP are essential components of the myelin sheath, playing crucial roles in maintaining its structure and functionality. It is noteworthy that MBP-deficient mice exhibit reduced myelin formation, and the myelin that does develop is characterized by loosely packed layers (Meschkat et al. 2022; Snaidero et al. 2014). Similarly, mice deficient in CNP display progressive axonal abnormalities, characterized by axonal swellings and spheroids, as well as widespread neurodegeneration across the brain (Lappe-Siefke et al. 2003; Snaidero et al. 2017). Therefore, a hypothesis could be that the increase in PLP protein levels due to its decreased autophagic degradation also affects MBP and CNP protein levels, resulting in myelin disorganization and decompaction.

Furthermore, we performed behavioral tests to discern potential functional implications of autophagy ablation in OLs. Changes in behavior were observed in the novel object recognition test, where aged cKO mice displayed inferior performance compared to aged control mice. This alteration may suggest a role for autophagy in myelin plasticity, essential for memory and learning abilities (Bonetto et al. 2021). MRI studies have shown that acquiring new motor skills or cognitive abilities results in changes in white matter pathways, reflecting the refinement of neural circuits (Scholz et al. 2009). Similarly, rats engaged in motor learning tasks show increased fractional anisotropy in MRI scans (Sampaio-Baptista et al. 2013). Therefore, autophagy depletion in OLs may lead to myelin remodeling effects, influencing cognitive behaviors such as learning and memory. In temporal order- and object-location recognition tests, aged cKO mice performed similarly to aged control mice, suggesting no significant impairments in these cognitive domains. Notably, although controls tended to perform better in the object-location test, this effect was not statistically significant. It is suggested that the neural circuitry for recognition memory differs among various types of memory. Specifically, the temporal-order object-recognition task is considered a prefrontal cortex (PFC)-dependent task that evaluates recency memory, while the novel object-recognition task and the object-location recognition tasks are primarily dependent on the perirhinal cortex and hippocampus, respectively, rather than the PFC (Barker et al. 2007; Warburton and Brown 2015). Thus, considering all the above and the main alterations observed in the novel object test, we can speculate that myelin turnover and remodeling may be more critical for the hippocampus and possibly the perirhinal cortex than for the PFC, at least during aging.

Other than the cognitive tests, we analyzed motor behavior and did not find motor deficits that could be correlated with the lack of changes in myelin proteins in the cerebral cortex in aged cKO (Figure S1). It is interesting to note that the somatosensory cortex continues myelinating and shows age-related decline only after 35 months of age (Hill et al. 2018; Hughes et al. 2018).

Concomitantly, we examined the distribution of OL lineage cell populations in aged mice and controls. Quantification of OPCs and mature OLs showed no significant differences between control and cKO genotypes. However, interestingly, an increased intensity of Iba1, as well as of CD11b, was observed in aged cKO mice. This elevation could reflect microglial activation, indicating that in the case of autophagic blockage in OLs, microglia may be more responsive to degrade excessive or damaged myelin. Thus, it is plausible to consider a parallel or complementary function between microglia and autophagy in the context of CNS myelin degradation during aging. While microglia might be responsible for identifying and initiating the removal of myelin debris, autophagy within OLs could aid in the efficient breakdown of excess myelin components, ensuring a finely tuned myelination process and optimizing neural connectivity as the CNS matures. This observation highlights the complex interplay between autophagy disruption, OL function, and the potential involvement of the immune response in maintaining myelin homeostasis.

Overall, depletion of autophagy in OLs in vivo led to significant morphological defects in the myelin membrane, increased axonal degeneration, accompanied by behavioral deficits in aged mice. The observed phenotype in autophagy-ablated aged mice could result from an accumulation of surplus myelin that cannot be degraded during development (as indicated by PLP protein accumulation, Ktena et al. 2022 and here), thereby disrupting the balance between myelin replenishment and degradation. Our study suggests that autophagy likely facilitates myelin turnover,

where new membranes replace older ones, necessitating the removal of the latter (Meschkat et al. 2022; Sampaio-Baptista and Johansen-Berg 2017). Recent data indicate that the elimination of abnormally deposited myelin, whether due to trauma or developmental turnover, involves microglia-mediated phagocytosis and astrocyte-mediated endocytosis (Djannatian et al. 2023; Hughes and Appel 2020; Ponath et al. 2017). We propose that, in addition to these mechanisms, autophagy within OLs could play a role in clearing CNS myelin deposits under steady-state conditions, maintaining the balance between replenishment and degradation, which might also impact axonal integrity, not only during adulthood as previously shown by our group and others (Ktena et al. 2022; Aber et al. 2022), but also during aging. Finally, the increased microglia activation in the case of autophagic ablation in OLs proposes that autophagy in OLs and microgliosis might work together to compensate for myelin degradation and clearance during aging. Overall, this research provides new insights into the role of autophagy in OLs, proposing it is an essential mechanism for CNS myelin maintenance and degradation, as well as axonal integrity, in aging.

Author Contributions

N.K. designed and performed experiments, analyzed data, and wrote the manuscript. A.G., D.S., I.K., E.T., and A.K. performed experiments and analyzed data. V.N. and M.S. designed experiments and edited the manuscript. D.K. designed and supervised experiments and analysis and edited the manuscript.

Acknowledgments

We are thankful to Prof. Kyriaki Sidiropoulou for her help and advice in the behavioral analysis and for constructive comments on the manuscript, Dr. Christel Genoud and Dr. Wei Jiao for electron microscopy support. This work was supported by funding from the Hellenic Foundation for Research and Innovation (HFRI grant agreements 1676 [to M.S.] and 14772 [to D.K.]), the National Recovery and Resilience Plan Greece 2.0, funded by the European Union—Next Generation EU, Proposal TAEDR 0535850 (to D.K.), the National Multiple Sclerosis Society (NMSS, pilot Research Grant, PP-1809-32556 to M.S.), the State Scholarships Foundation (IKY, in the context of the project "Strengthening Human Resources Research Potential via Doctorate Research", MIS-5113934), the Hellenic Academy of Neuroimmunology (HELANI) and the Manassaki scholarship of the University of Crete (to N.K.). Furthermore, we would like to state that cartoons in Figures 1A, 3, and S4, and the graphical abstract were created with BioRender.com.

Ethics Statement

The animal study was reviewed and approved by the Animal Facility of the Institute of Molecular Biology and Biotechnology (IMBB)-Foundation for Research and Technology Hellas (FORTH) (license nos. EL91-BIObr-01 and EL91-BIOexp-02) which complies with all regulations and standards outlined in the Presidential Decree 56/30.04.2013 (Greek Law). All procedures were performed in accordance with the EU directives and regulations (2010/63/EU and L 276/33/20.10.2010) that are equivalent to NIH standards established by the Animal Welfare Acts and the documents entitled "Principles for Use of Animals" and "Guide for the Care and Use of Laboratory Animals" from the Office of Laboratory Animal Welfare. Experimental animal protocols have been approved with license number 93164 (A1A: 73XB7 ΛΚ-ΦΙΣ).

Consent

The authors have nothing to report.

Conflicts of Interest

The authors declare no conflicts of interest.

Data Availability Statement

The data that support the findings of this study are available from the corresponding author upon reasonable request.

References

Aber, E. R., C. J. Griffey, T. Davies, et al. 2022. "Oligodendroglial Macroautophagy Is Essential for Myelin Sheath Turnover to Prevent Neurodegeneration and Death." *Cell Reports* 41: 111480.

Aman, Y., T. Schmauck-Medina, M. Hansen, et al. 2021. "Autophagy in Healthy Aging and Disease." *Nature Aging* 1: 634–650.

Anderson, T. J., A. Schneider, J. A. Barrie, et al. 1998. "Late-Onset Neurodegeneration in Mice With Increased Dosage of the Proteolipid Protein Gene." *Journal of Comparative Neurology* 394: 506–519.

Bankston, A. N., M. D. Forston, R. M. Howard, et al. 2019. "Autophagy Is Essential for Oligodendrocyte Differentiation, Survival, and Proper Myelination." *Glia* 67: 1745–1759.

Barker, G. R., F. Bird, V. Alexander, and E. C. Warburton. 2007. "Recognition Memory for Objects, Place, and Temporal Order: A Disconnection Analysis of the Role of the Medial Prefrontal Cortex and Perirhinal Cortex." *Journal of Neuroscience* 27: 2948–2957.

Bartzokis, G. 2004. "Age-Related Myelin Breakdown: A Developmental Model of Cognitive Decline and Alzheimer's Disease." *Neurobiology of Aging* 25: 5–18.

Bartzokis, G. 2011. "Alzheimer's Disease as Homeostatic Responses to Age-Related Myelin Breakdown." *Neurobiology of Aging* 32: 1341–1371.

Bartzokis, G., J. L. Cummings, D. Sultzer, V. W. Henderson, K. H. Nuechterlein, and J. Mintz. 2003. "White Matter Structural Integrity in Healthy Aging Adults and Patients With Alzheimer Disease: A Magnetic Resonance Imaging Study." *Archives of Neurology* 60: 393–398.

Bartzokis, G., P. H. Lu, K. Tingus, et al. 2010. "Lifespan Trajectory of Myelin Integrity and Maximum Motor Speed." *Neurobiology of Aging* 31: 1554–1562.

Bartzokis, G., P. H. Lu, T. A. Tishler, et al. 2007. "Myelin Breakdown and Iron Changes in Huntington's Disease: Pathogenesis and Treatment Implications." *Neurochemical Research* 32: 1655–1664.

Bonetto, G., D. Belin, and R. T. Karadottir. 2021. "Myelin: A Gatekeeper of Activity-Dependent Circuit Plasticity?" *Science* 374: eaba6905.

Casella, C., I. Lipp, A. Rosser, D. K. Jones, and C. Metzler-Baddeley. 2020. "A Critical Review of White Matter Changes in Huntington's Disease." *Movement Disorders* 35: 1302–1311.

Clark, R. E., S. M. Zola, and L. R. Squire. 2000. "Impaired Recognition Memory in Rats After Damage to the Hippocampus." *Journal of Neurosci.ence* 20: 8853–8860.

Costa, R. M., D. Cohen, and M. A. Nicolelis. 2004. "Differential Corticostriatal Plasticity During Fast and Slow Motor Skill Learning in Mice." *Current Biology* 14: 1124–1134.

de Faria, O., Jr., H. Pivonkova, B. Varga, S. Timmler, K. A. Evans, and R. T. Karadottir. 2021. "Periods of Synchronized Myelin Changes Shape Brain Function and Plasticity." *Nature Neuroscience* 24: 1508–1521.

Dean, D. C., J. Sojkova, S. Hurley, et al. 2016. "Alterations of Myelin Content in Parkinson's Disease: A Cross-Sectional Neuroimaging Study." *PLoS One* 11: e0163774.

Dean, D. C., S. A. Hurley, S. R. Kecskemeti, et al. 2017. "Association of Amyloid Pathology With Myelin Alteration in Preclinical Alzheimer

Disease." *JAMA Neurology* 74, no. 1: 41–49. https://doi.org/10.1001/jamaneurol.2016.3232.

Depp, C., T. Sun, A. O. Sasmita, et al. 2023. "Myelin Dysfunction Drives Amyloid-Beta Deposition in Models of Alzheimer's Disease." *Nature* 618: 349–357.

Dere, E., J. P. Huston, and M. A. De Souza Silva. 2007. "The Pharmacology, Neuroanatomy and Neurogenetics of One-Trial Object Recognition in Rodents." *Neuroscience and Biobehavioral Reviews* 31: 673–704.

Djannatian, M., S. Radha, U. Weikert, et al. 2023. "Myelination Generates Aberrant Ultrastructure That Is Resolved by Microglia." *Journal of Cell Biology* 222, no. 3: e202204010.

Ennaceur, A., and J. P. Aggleton. 1997. "The Effects of Neurotoxic Lesions of the Perirhinal Cortex Combined to Fornix Transection on Object Recognition Memory in the Rat." *Behavioural Brain Research* 88: 181–193.

Galvez-Contreras, A. Y., D. Zarate-Lopez, A. L. Torres-Chavez, and O. Gonzalez-Perez. 2020. "Role of Oligodendrocytes and Myelin in the Pathophysiology of Autism Spectrum Disorder." *Brain Sciences* 10, no. 12: 951. https://doi.org/10.3390/brainsci10120951.

Hammad, M., A. Silva, J. Glass, J. T. Sladky, and M. Benatar. 2007. "Clinical, Electrophysiologic, and Pathologic Evidence for Sensory Abnormalities in ALS." *Neurology* 69: 2236–2242.

Hara, T., K. Nakamura, M. Matsui, et al. 2006. "Suppression of Basal Autophagy in Neural Cells Causes Neurodegenerative Disease in Mice." *Nature* 441, no. 7095: 885–889. https://doi.org/10.1038/nature04724.

Hill, R. A., A. M. Li, and J. Grutzendler. 2018. "Lifelong Cortical Myelin Plasticity and Age-Related Degeneration in the Live Mammalian Brain." *Nature Neuroscience* 21: 683–695.

Hughes, A. N., and B. Appel. 2020. "Microglia Phagocytose Myelin Sheaths to Modify Developmental Myelination." *Nature Neuroscience* 23: 1055–1066.

Hughes, E. G., J. L. Orthmann-Murphy, A. J. Langseth, and D. E. Bergles. 2018. "Myelin Remodeling Through Experience-Dependent Oligodendrogenesis in the Adult Somatosensory Cortex." *Nature Neuroscience* 21: 696–706.

Ip, C. W., A. Kroner, M. Bendszus, et al. 2006. "Immune Cells Contribute to Myelin Degeneration and Axonopathic Changes in Mice Overexpressing Proteolipid Protein in Oligodendrocytes." *Journal of Neuroscience* 26: 8206–8216.

Jimenez-Loygorri, J. I., B. Villarejo-Zori, A. Viedma-Poyatos, et al. 2024. "Mitophagy Curtails Cytosolic mtDNA-Dependent Activation of cGAS/STING Inflammation During Aging." *Nature Communications* 15: 830.

Kallergi, E., and V. Nikoletopoulou. 2021. "Macroautophagy and Normal Aging of the Nervous System: Lessons From Animal Models." *Cell Stress* 5: 146–166.

Kallergi, E., D. Siva Sankar, A. Matera, et al. 2023. "Profiling of Purified Autophagic Vesicle Degradome in the Maturing and Aging Brain." *Neuron* 111: 2329–2347.e7.

Kang, S. H., Y. Li, M. Fukaya, et al. 2013. "Degeneration and Impaired Regeneration of Gray Matter Oligodendrocytes in Amyotrophic Lateral Sclerosis." *Nature Neuroscience* 16: 571–579.

Karim, S. A., J. A. Barrie, M. C. McCulloch, et al. 2007. "PLP Overexpression Perturbs Myelin Protein Composition and Myelination in a Mouse Model of Pelizaeus-Merzbacher Disease." *Glia* 55: 341–351.

Kolotuev, I. 2014. "Positional Correlative Anatomy of Invertebrate Model Organisms Increases Efficiency of TEM Data Production." *Microscopy and Microanalysis* 20: 1392–1403.

Kremer, J. R., D. N. Mastronarde, and J. R. McIntosh. 1996. "Computer Visualization of Three-Dimensional Image Data Using IMOD." *Journal of Structural Biology* 116: 71–76.

Ktena, N., S. I. Kaplanis, I. Kolotuev, et al. 2022. "Autophagic Degradation of CNS Myelin Maintains Axon Integrity." *Cell Stress* 6: 93–107.

Lappe-Siefke, C., S. Goebbels, M. Gravel, et al. 2003. "Disruption of Cnp1 Uncouples Oligodendroglial Functions in Axonal Support and Myelination." *Nature Genetics* 33: 366–374.

Laukka, J. J., J. Kamholz, D. Bessert, and R. P. Skoff. 2016. "Novel Pathologic Findings in Patients With Pelizaeus-Merzbacher Disease." *Neuroscience Letters* 627: 222–232.

Leone, D. P., S. Genoud, S. Atanasoski, et al. 2003. "Tamoxifen-Inducible Glia-Specific Cre Mice for Somatic Mutagenesis in Oligodendrocytes and Schwann Cells." *Molecular and Cellular Neurosciences* 22: 430–440.

Lintl, P., and H. Braak. 1983. "Loss of Intracortical Myelinated Fibers: A Distinctive Age-Related Alteration in the Human Striate Area." *Acta Neuropathologica* 61: 178–182.

Marner, L., J. R. Nyengaard, Y. Tang, and B. Pakkenberg. 2003. "Marked Loss of Myelinated Nerve Fibers in the Human Brain With Age." *Journal of Comparative Neurology* 462: 144–152.

Mathys, H., J. Davila-Velderrain, Z. Peng, et al. 2019. "Single-Cell Transcriptomic Analysis of Alzheimer's Disease." *Nature* 570: 332–337.

McKenzie, I. A., D. Ohayon, H. Li, et al. 2014. "Motor Skill Learning Requires Active Central Myelination." *Science* 346: 318–322.

Menzies, F. M., A. Fleming, A. Caricasole, et al. 2017. "Autophagy and Neurodegeneration: Pathogenic Mechanisms and Therapeutic Opportunities." *Neuron* 93: 1015–1034.

Meschkat, M., A. M. Steyer, M. T. Weil, et al. 2022. "White Matter Integrity in Mice Requires Continuous Myelin Synthesis at the Inner Tongue." *Nature Communications* 13: 1163.

Mitchell, J. B., and J. Laiacona. 1998. "The Medial Frontal Cortex and Temporal Memory: Tests Using Spontaneous Exploratory Behaviour in the Rat." *Behavioural Brain Research* 97: 107–113.

Munoz-Galdeano, T., D. Reigada, A. Del Aguila, et al. 2018. "Cell Specific Changes of Autophagy in a Mouse Model of Contusive Spinal Cord Injury." *Frontiers in Cellular Neuroscience* 12: 164.

Nutma, E., M. C. Marzin, S. A. Cillessen, and S. Amor. 2021. "Autophagy in White Matter Disorders of the CNS: Mechanisms and Therapeutic Opportunities." *Journal of Pathology* 253: 133–147.

Pan, S., S. R. Mayoral, H. S. Choi, J. R. Chan, and M. A. Kheirbek. 2020. "Preservation of a Remote Fear Memory Requires New Myelin Formation." *Nature Neuroscience* 23: 487–499.

Pasquettaz, R., I. Kolotuev, A. Rohrbach, C. Gouelle, L. Pellerin, and F. Langlet. 2021. "Peculiar Protrusions Along Tanycyte Processes Face Diverse Neural and Nonneural Cell Types in the Hypothalamic Parenchyma." *Journal of Comparative Neurology* 529: 553–575.

Perge, J. A., J. E. Niven, E. Mugnaini, V. Balasubramanian, and P. Sterling. 2012. "Why do Axons Differ in Caliber?" *Journal of Neuroscience* 32, no. 2: 626–638.

Pernet, V., S. Joly, F. Christ, L. Dimou, and M. E. Schwab. 2008. "Nogo-A and Myelin-Associated Glycoprotein Differently Regulate Oligodendrocyte Maturation and Myelin Formation." *Journal of Neuroscience* 28, no. 29: 7435–7444.

Peters, A. 2002. "The Effects of Normal Aging on Myelin and Nerve Fibers: A Review." *Journal of Neurocytology* 31: 581–593.

Peters, A. 2009. "The Effects of Normal Aging on Myelinated Nerve Fibers in Monkey Central Nervous System." *Frontiers in Neuroanatomy* 3: 11.

Ponath, G., S. Ramanan, M. Mubarak, et al. 2017. "Myelin Phagocytosis by Astrocytes After Myelin Damage Promotes Lesion Pathology." *Brain* 140: 399–413.

Pyo, J. O., S. M. Yoo, H. H. Ahn, et al. 2013. "Overexpression of Atg5 in Mice Activates Autophagy and Extends Lifespan." *Nature Communications* 4: 2300.

Rodriguez-Diehl, R., D. Vilas, N. Bargallo, E. Tolosa, and E. Gelpi. 2019. "Co-Morbid Demyelinating Lesions and Atypical Clinical Features in

a Patient With Parkinson's Disease." *Parkinsonism & Related Disorders* 62: 242–245.

Roy, A., Y. K. Fung, X. Liu, and K. Pahan. 2006. "Up-Regulation of Microglial CD11b Expression by Nitric Oxide." *Journal of Biological Chemistry* 281: 14971–14980.

Safaiyan, S., N. Kannaiyan, N. Snaidero, et al. 2016. "Age-Related Myelin Degradation Burdens the Clearance Function of Microglia During Aging." *Nature Neuroscience* 19: 995–998.

Salat, D. H., D. S. Tuch, D. N. Greve, et al. 2005. "Age-Related Alterations in White Matter Microstructure Measured by Diffusion Tensor Imaging." *Neurobiology of Aging* 26, no. 8: 1215–1227. https://doi.org/10.1016/j.neurobiolaging.2004.09.017.

Sampaio-Baptista, C., A. A. Khrapitchev, S. Foxley, et al. 2013. "Motor Skill Learning Induces Changes in White Matter Microstructure and Myelination." *Journal of Neuroscience* 33: 19499–19503.

Sampaio-Baptista, C., and H. Johansen-Berg. 2017. "White Matter Plasticity in the Adult Brain." *Neuron* 96: 1239–1251.

Saraswat Ohri, S., A. N. Bankston, S. A. Mullins, et al. 2018. "Blocking Autophagy in Oligodendrocytes Limits Functional Recovery After Spinal Cord Injury." *Journal of Neuroscience* 38: 5900–5912.

Scholz, J., M. C. Klein, T. E. Behrens, and H. Johansen-Berg. 2009. "Training Induces Changes in White-Matter Architecture." *Nature Neuroscience* 12: 1370–1371.

Snaidero, N., C. Velte, M. Myllykoski, et al. 2017. "Antagonistic Functions of MBP and CNP Establish Cytosolic Channels in CNS Myelin." *Cell Reports* 18: 314–323.

Snaidero, N., W. Mobius, T. Czopka, et al. 2014. "Myelin Membrane Wrapping of CNS Axons by PI(3,4,5)P3-Dependent Polarized Growth at the Inner Tongue." *Cell* 156, no. 1-2: 277–290. https://doi.org/10.1016/j.cell.2013.11.044.

Stassart, R. M., W. Mobius, K. A. Nave, and J. M. Edgar. 2018. "The Axon-Myelin Unit in Development and Degenerative Disease." *Frontiers in Neuroscience* 12: 467.

Steadman, P. E., F. Xia, M. Ahmed, et al. 2020. "Disruption of Oligodendrogenesis Impairs Memory Consolidation in Adult Mice." *Neuron* 105: 150–164.e6.

Stedehouder, J., and S. A. Kushner. 2017. "Myelination of Parvalbumin Interneurons: A Parsimonious Locus of Pathophysiological Convergence in Schizophrenia." *Molecular Psychiatry* 22: 4–12.

Tang, Y., J. R. Nyengaard, B. Pakkenberg, and H. J. Gundersen. 1997. "Age-Induced White Matter Changes in the Human Brain: A Stereological Investigation." *Neurobiology of Aging* 18: 609–615.

Tripathi, R. B., M. Jackiewicz, I. A. McKenzie, E. Kougioumtzidou, M. Grist, and W. D. Richardson. 2017. "Remarkable Stability of Myelinating Oligodendrocytes in Mice." *Cell Reports* 21: 316–323.

Warburton, E. C., and M. W. Brown. 2015. "Neural Circuitry for Rat Recognition Memory." *Behavioural Brain Research* 285: 131–139.

Xekardaki, A., P. Giannakopoulos, and S. Haller. 2011. "White Matter Changes in Bipolar Disorder, Alzheimer Disease, and Mild Cognitive Impairment: New Insights From DTI." *Journal of Aging Research* 2011: 286564.

Yang, K., Z. Wu, J. Long, et al. 2023. "White Matter Changes in Parkinson's Disease." *npj Parkinson's Disease* 9: 150.

Supporting Information

Additional supporting information can be found online in the Supporting Information section.